IEEE Access
Multidisciplinary | Rapid Review | Open Access Journal

Received February 4, 2022, accepted February 27, 2022, date of publication March 2, 2022, date of current version March 18, 2022.

Digital Object Identifier 10.1109/ACCESS.2022.3156113

Optical Modeling and Characterization of Demyelinated Nerve Using Graphene-Based Photonic Structure

AMIR MAGHOUL[1,2], ALI ROSTAMI[2], MLADEN VELETIĆ[1,3], BIGE DENIZ UNLUTURK[4], (Member, IEEE), NILOJAN GNANAKULASEKARAN[3], AND ILANGKO BALASINGHAM[1,3], (Senior Member, IEEE)

[1]Department of Electronic Systems, Norwegian University of Science and Technology, 7491 Trondheim, Norway
[2]Photonics and Nanocrystal Research Laboratory (PRNL), Faculty of Electrical and Computer Engineering, University of Tabriz, Tabriz 5166614761, Iran
[3]Intervention Center, Oslo University Hospital, 0027 Oslo, Norway
[4]Institute of Quantitative Health Science and Engineering, Michigan State University, East Lansing, MI 48824, USA

Corresponding author: Amir Maghoul (amaghoul@tabrizu.ac.ir; amnano91@gmail.com)

This work was supported in part by the European Research Consortium for Informatics and Mathematics (ERCIM), and in part by the Research Council of Norway Funded Project CIRCLE under Grant 287112.

ABSTRACT The myelin sheath, as an insulation layer in nerve cells, plays an essential role in neural communication and signal conduction. Loss of myelin, referred to as demyelination, is associated with many mental disorders. Detecting the tiny demyelinated parts in nerve fibers can provide early diagnosis of some mental disorders and create effective treatment plans. This paper establishes a new engineering approach for differentiation between demyelinated and myelinated axons by analyzing spectral responses resulting from the optical simulation framework. We propose computational modeling on the photonic communication of nerve fibers and develop a graphene-based neurophotonic device that can be used to detect the regions demyelinated on the nerve fiber. We first model a nanoscale thin-film configuration of the multilayered myelinated axon to evaluate photons transmission in the nerve fibers under geometric defects as demyelination. Then, the nerve's optical characteristics are achieved by focusing on the reflectance of light incidence on the nerve model with the change of the demyelination size to distinguish demyelinated—from myelinated nerves by the spectral contrast. Undertaking the different levels of demyelination progression, we theoretically explore the variations of effective refractive index using an analytical solution technique. Ultimately, we design a nanostructure configured with silicon dioxide, graphene, and gold nanoparticles to function as a biochip recognizing myelinated axon damage under the surface plasmon effect. This device can promote a practical procedure to distinguish nanoscale demyelinated and myelinated axons, which can be utilized for neural sensing of tiny brain tissues as a neurophotonic needle.

INDEX TERMS Multilayered myelinated axon, demyelination, photonic communication, effective refractive index, graphene layer, gold nanoparticle.

I. INTRODUCTION

Intra-extracellular signaling between neurons is an essential function of the human brain that is vital to survival [1], [2]. Nerve fibers serve as connection channels in a neuronal communication network to transmit bio-information between nerve cells in the body. Almost every 100 billion nerve cells in the human brain are connected to 10 thousand others on average through a great nerve fiber network to support cell-to-cell communications [3], [4]. The nerve fibers, which are a suitable platform for nerve signal transmission, comprise two main parts: myelin sheath and axon; the myelin sheath formed around the axon in multilayered configuration functions as an insulator to sustain the conduction of neural signal inside the nerve fiber [5]–[8]. The myelin sheath's pathway has the potential to conduct a propagating phenomenon called action potential (AP) based on a sharp variation of electrical potential across the interior and exterior of the cell membrane [9], [10]. The conduction speed of AP in the myelinated axon can be significantly enhanced

The associate editor coordinating the review of this manuscript and approving it for publication was Lin Lin.

compared to that in the unmyelinated axons due to the ''saltatory conduction'' process [11], [12]. Generating and thickening myelin sheath also impacts learning new skills and memory [13], [14]. Further, defects in the myelin sheath cause various brain disorders, including stroke, spinal cord injury, and multiple sclerosis (MS). In the case of MS, the body's immune system attacks the myelin sheath of nerves and damages it [15]. Fig.1 shows a graphic configuration of a nerve fiber in which AP conduction through myelin sheath is highlighted schematically.

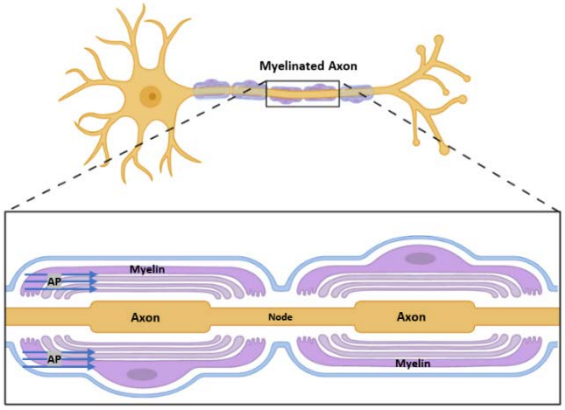

FIGURE 1. A schematic diagram of myelinated axon in the nerve fiber.

Demyelination of nerve fibers also leads to losing nerve pulses in the central nervous system, and a discontinuity in signaling may result in cell death [16], [17]. Detecting the tiny level of demyelination on the nerve fiber before progression can lead to early diagnosis of some mental disorders and help for prevention of disease development using effective drug plans. Thus, a promising procedure for identifying the demyelinated fibers can be approached as an early recognition and diagnosis paradigm. Based on the influential role of the myelin sheath during neuronal activities, the potential to monitor the myelinated axon status—determining whether it is normal or defective — can impressively affect the nervous system stimulation [18]. Employing electrical signals for nerve stimulation in the brain is very common; however, this method is inefficient for micro/nanoscale brain tissue because of incompatibility between wavelengths in kHz and sample size [19], [20]. By focusing on deep brain stimulation, particular mechanisms have emerged that deal with the implications of light manipulations for neural communication applications — optogenetic [21], upconversion techniques [22], [23], photon communication [24]–[26]—ranging from Terahertz (THz) to the optical frequencies [19], [27]. Modern optical techniques used to obtain a wavelength range corresponding to the thickness of myelin to virtualize a multilayer myelin nanostructure are being developed as part of breakthrough new knowledge in the field of neurophotonics [18]–[20], [28].

Recent studies have also provided more evidence for biochemical reactions, ion-transmembrane, and energy level transition of biomolecular activities in neuronal tissues that can produce biophotons in mediating intra-extracellular communication, which may affect the photonic signal transmission in the myelinated axons [29], [30].

In this article, photonic communication based on the nerve's thin-film model is investigated. For this, we assume that photons are available in forms other than being natural or human-made, and the myelin sheath's layers are considered the route for passing photonic signals in the nervous system network. The myelinated axon channel's transmittance is thereby achieved to evaluate the feasibility of photonic signal conduction in the myelinated axon with multilayered myelin. The impact of demyelination on transmittance is also calculated under a changing physical size of the defected area upon the myelin's layers. Thus, the reflectance spectra of myelinated axons with stacked myelin layers under external light irradiation are analyzed to explore the optical contrasts arising from demyelination's presence on the configured nerve model. In attempting to understand the achieved results, the modal index (effective refractive index) is obtained by an exact solution method derived from the calculated scattering coefficients. Keeping this in mind, we propose a new framework to build up biochips based on graphene materials for separation between myelinated and demyelinated nerves; the designed setup is established by focusing on the relationship between the modal index and plasmonic modes, which is depicted in detail. All simulations are carried out using a full-wave electromagnetic solver in CST Microwave Studio.

II. STRUCTURAL MODEL

From a morphological standpoint, the axon is configured with myelin layers surrounding separated at 1μm intervals known as ''nodes of Ranvier'' [31]. In the vertebrate nervous system, most axons covered by myelin are composed of nonpolar phospholipid-rich inserted as a multilayer sheath [32]. As such, the myelin sheath conducts action potentials (APs) rooted in the interaction between ions in nervous cell environments. From an electrical perspective, propagation of neural information in the myelin sheath results from action potential at the Ranvier node, and the salutatory phenomenon can be approximated as a metal cable based on Hodgkin Huxley's model [33]. However, this model is elementary, and many biophysical phenomena are ignored in that model [19]. On the other hand, exploring the myelin layers enwrapping the axon and the optical spectroscopy exhibit a multilayer configuration of myelin sheath with nanoscale precision [18]. In this way, access to the nanostructural dynamics of the myelin sheath can promote new applications in regard to the detection of a damaged myelinated axon which may have a significant effect on Alzheimer's and MS patients [34], [35]. Schain *et al.* [36] suggested a spectral reflectometry mechanism titled SCoRe in which high-contrast imaging of the myelinated axon is investigated via spectral reflectance from nerve tissues. The physical concepts of technique have been established by a multilayer thin-film stacked theory widely applied to design semiconductor electronic devices [37]. Kwon *et al.* [18] also reported a thin-film model of

myelinated axons associated with refractive indexes and the thickness of myelin gradients measured in a mouse brain via transmission electron microscopy (TEM) in visible range between 400nm and 700nm.

Moreover, a hypothesis is that photons can be transferred through the myelin sheath and can function as an optical waveguide, despite some challenges on the photon's source, whether it is human-made or natural. Recent findings also support the assumption that the myelin pathway of nerve fiber has the potential to pass the photons; however, those indications are based on only theoretical simulations and lack supporting experimental data [24], [27]. On this basis, the demyelination effect of nerve fibers can be considered interesting research in photonic communication in nerves. Fig.2(a) and (b) demonstrate a schematic of the myelinated and demyelinated axon. Fig.2 (c) further illustrates a cross-sectional view of the nerve fiber along with optical properties of myelin's layer described comprehensively in the next section.

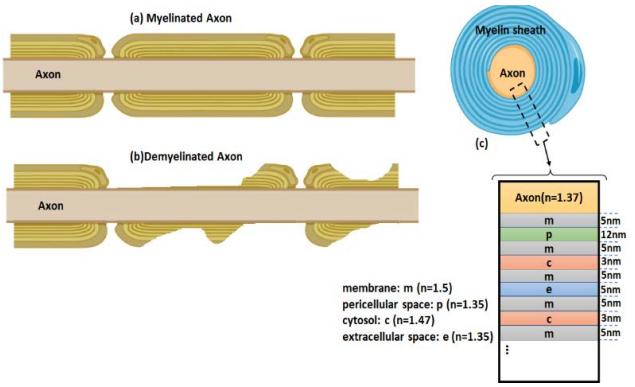

FIGURE 2. Illustration of (a) normal myelinated axon, (b) demyelinated axon, (c) a cross-sectional view of normal myelin axon with the myelins' ingredients associated with refractive index.

III. SIMULATION RESULTS

A. PHOTONIC SIGNALING INSIDE MULTILAYER MYELINATED AND DEMYELINATED AXON

Myelinated axons are thought to be the communication links between neurons that enable the transmission of bio-information in the nervous network system. As mentioned earlier, the myelin part of the nerve segment operates as an insulator, forming fatty layers around the axon. First, we need to provide a model of the myelinated axon for our simulations. We thus choose a thin-film model of a myelinated axon via a nanostructural dynamics structure of the nerves. As another point about the nerve model configured, we consider the multilayered myelinated axon without random variance in shape and some irregularities, which can affect the physics of the problem by altering electromagnetic modal features under interaction with an ongoing wave. It can also be considered as a future outlook of our work. Due to avoiding the massive processing volume, complexity in computations, and probability of simulation error, we neglect geometrical irregularities in the CAD implementation of the nerve model. However, we utilize a structural model of the myelinated axon arising from experimental and practical tests, which have been resulted in [18], [38]. According to this model, the myelin is composed of the membrane, cytosol, extracellular space, and pericellular space layered on each other, as illustrated in Fig. 2(c). The refractive index of each layer is shown in Fig.2(c). Due to the absence of data related to refractive index in the desired range, especially ultraviolet (UV), and also minor variations of the real part of refractive index in the NIR range [39], we consider the refractive index of the thin-film model of nerve fiber reported in [18] for the whole of the desired wavelength band in this work. Furthermore, the axon's diameter and the myelin thickness are equal to 0.46μm and 0.112μm, respectively [40]. Notably, a 5-μm length of the myelinated axon is considered in our work.

Given the size of the myelin's layers in the modeled structure and their nanoscale dynamics, the simulations were carried out in a wide range of wavelengths, including UV-visible and near-infrared (NIR) between 100 nm and 1μm. By focusing on the myelin's waveguide potential and assuming that photons can pass through the myelin pathway, the multilayer myelinated axon's transmittance is simulated. Fig.3(a) and (b) demonstrate the multilayer myelinated axon structure implemented in the CST Microwave Suite. To further clarify, a demonstration of refractive index variations with respect to the radial distance of the rectangular solid core nerve fiber is shown in Fig.3 (c).

To assess the performance of implemented nerve model, the transmittance parameter of the nerve model is calculated. Transmittance is the relationship between the amount of light is transmitted (I_T) to the thin film nerve once it has passed through the model and the original amount of light (I_0), which is defined by [41]:

$$T_{(dB)} = 10.\log(\frac{I_T}{I_0}) \tag{1}$$

At first, to investigate the coupling effect of the incoming signal in the axon and myelin sheath, the guided photonic signal strength inside the multilayered myelinated axon is simulated by placing the output in the axon and myelin layers on the other side We choose a waveguide port for applying excitation signal in myelin sheath as input in the software environment, as can be seen in Fig.3(b). Then, another waveguide port is placed on the myelin layers and axon at each turn as output. We use a mesh setting with the smallest cell of 2.5 nm and the largest cell 4.81 nm, which includes more than 100 million mesh cells upon the z coordinate axis, also suggested by default in the CAD environment for the meshing process of all simulations.

By applying an excitation signal within the myelin, photons are guided inside the myelinated axon's configuration. The simulation results reveal a significant peak in shorter wavelengths under 350nm in the myelin output's spectral response, as seen in Fig.4 (a). Also, there is a downward trend in the transmission band due to the existence of the cut-off wavelength in the higher wavelengths. As such, Fig.4 (b)

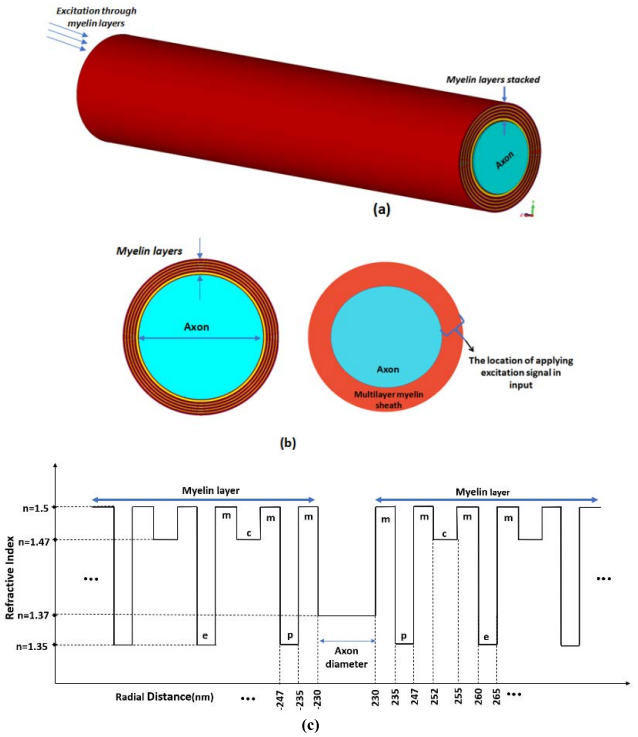

FIGURE 3. **(a) Myelinated axon implemented in CST Microwave Suite, (b) A cross-sectional view of CAD implementation and location of applying excitation signal in input (c) Refractive index variation with the radial distance of rectangular solid core nerve fiber based on nanoscale dynamic.**

shows that the coupling effect of the guided photonic signal inside the axon is negligible, and the myelin's layers contain photonic energy well because of their refractive indexes. In other words, the predominant role of the effective refractive index leads to more energy confinements in the myelin sheath; consequently, the transmittance becomes considerable in the myelin's output. Moreover, the forward reflectance available between the layers of the myelin sheath has the potential to create constructive interference stemming from phase matching of the generated electromagnetic modes in multilayer structures [42].

From an electro-optics perspective, the results indicate a resonance mode that occurs in the low wavelength of the transmission band with the myelin's output, rooted in the myelinated axon's multilayered structure, which has a performance similar to the circular multilayer waveguide [43]. The myelinated axon's spectral response illustrates that the ratio of stored energy to dissipated energy is dominant in the transmission band, resulting in a high-quality factor which means the resonance mode [44]. It is also interesting to know; the achieved resonance can change upon the transmission band under the impact of geometrical variance of nerve configuration due to altering modal characteristics [45] that can be followed up in the next works. Fig.4 (c), (d), (e), and (g) illustrate the electric field distribution in the middle of and across the modeled myelinated axon at wavelengths where the transmittance peaks over the transmission band with the axon and myelin outputs.

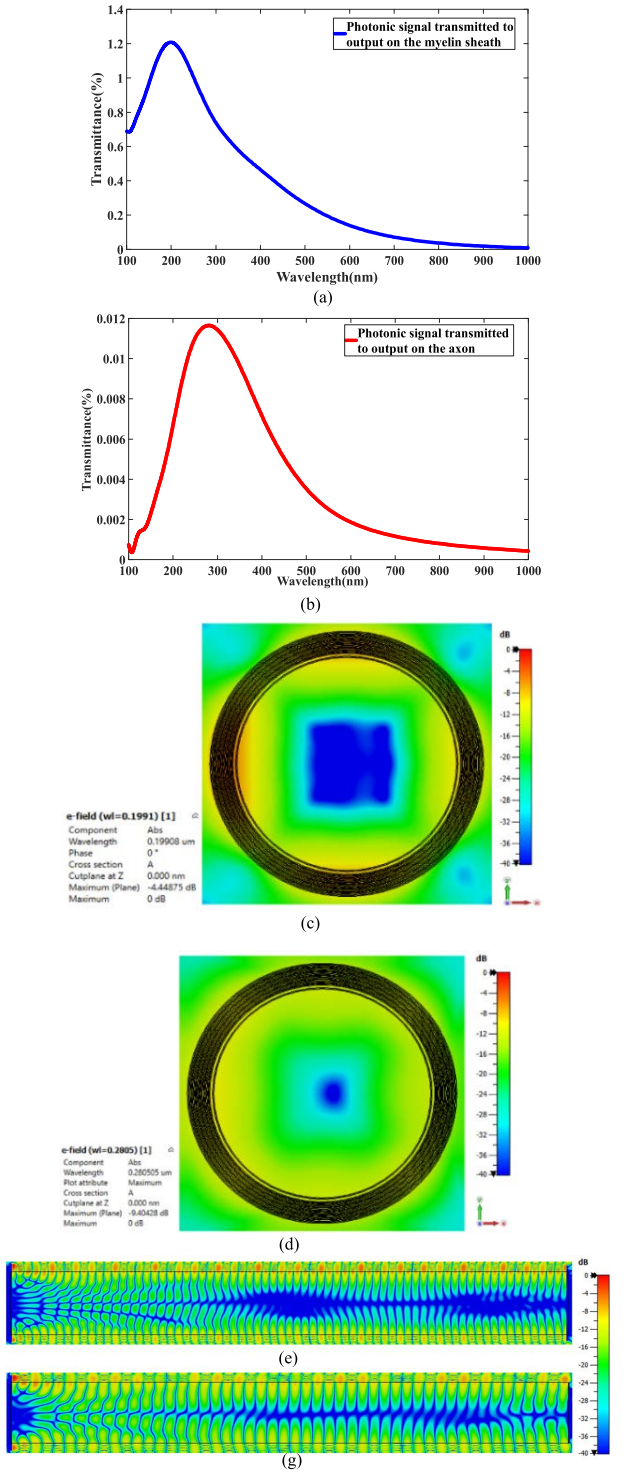

FIGURE 4. **Transmittance coefficient of a multilayer myelinated axon with (a) myelin sheath port, (b) axon port, (c) Electric field distribution in the middle of the considered myelinated axon at 199.08 nm with myelin output, (d) Electric field distribution in the middle of the considered myelinated axon at 280.5nm with axon output, (e) Electric field distribution across the myelinated axon model under stimulation of myelin layers at 199.08 nm with myelin output, (g) Electric field distribution across the myelinated axon model under stimulation of myelin layers at 280.5nm with axon output.**

In the following section, the effect of a myelinated axon defect, as demyelination, on the transmittance is investigated. The aim is to find the impact of demyelination on the photonic

signal passing within the myelin layers. Therefore, a demyelination part is created in the middle of the multilayer myelinated axon with a length of 1000 nm and depth of 112 nm. As a point of clarity, to investigate the absence impact of the myelin sheath as a part demyelinated on the myelinated axon, we consider a defection with a depth that is equal to the multilayered myelin's thickness in a length of 1000 nm across the nerve fiber as a primary assumption and start the simulations. In this regard, quantitive assessments and experimental tests have recently been reported as well [46]–[48].

The demyelinated area is assumed as a form of the semi-cylindrical sheath with a specific solid angle ($\theta = 90$ degrees), as demonstrated in Fig.5 (a), (b), and (c). First, the demyelination effect on the myelinated axon's transmittance is evaluated. As seen in Fig.5 (d), a considerable decrease in transmittance occurs over the transmission band of the demyelinated axon's spectral response under 350 nm. Contrasting the electric field distribution of the demyelinated axon with the normal myelinated axon in Fig.5(e) illustrates that the electric field components are dissipated under the impact of reflections created in the demyelination zone. In this state, more energy goes toward the axon rather than the extracellular medium because of the more refractive index value of the axon than the extracellular medium. In other words, reflections available in the demyelination site create a constructive interference of electromagnetic field components propagating in the axonal zone after the demyelination part in comparison with the normal myelinated axon. Indeed, the defection of the myelin sheath affects the configuration's modal index, resulting in a reduction of photonic communication inside the myelin sheath. In other words, demyelination manipulates the nerve fiber's electromagnetic modes, obstructing photon transition. Defection removes some of the guided modes of the electromagnetic wave in a demyelinated axon that causes attenuation in the received signal with the myelin's output. Besides, a redshift occurs in the spectral response, and the transmittance makes a forward shift towards the upper wavelengths under demyelination.

To gather more information, the impact of demyelination on photon transition in the myelin's layers is engineered. Hence, the demyelination architecture in terms of geometry is varied. The demyelinated area's size and the solid angle θ defined in Fig.5 (b), (c) are thereby changed. First, the length of the defected area (L) varies by 250 nm, 500 nm, 750 nm, 1250 nm, and 1500 nm, with the depth of demyelination fixed at 112nm. We consider these values due to evaluate the changes in the optical parameters of the multilayered myelinated axon model under the different levels of demyelination. The simulated results in Fig.5(f) indicate that the photonic transmission decreases with an increase in the length of demyelination under 400 nm in the transmission band, which is rooted in the removal of the guided modes due to diffraction in the defected location. Despite attenuation of resonant amplitude, we observe a significant redshift in the transmission band's resonant peak based on an increasing demyelination length.

Then, we concentrate on the depth effect of demyelination on the optical characteristic of modeled configuration. As determined from Fig.2 (c), the modeled myelin sheath comprises layers such as m, p, c, and e. Therefore, it is evident that a combination of the layers (m/c/m/e) can be considered as the main section of the thin-film model of a myelinated axon. On this basis, defections in the myelin sheath's depth are arranged by 23 nm, 41 nm, 59 nm, 77 nm, 95 nm, and 112 nm, including a mixture of the main layers and other sections of the myelin sheath such as 'p.' As expected, the simulated results in Fig.5(g) show that removing the myelin's layers causes lesser photonic signal transfer through the myelin sheath, which means that the defection on the layers damages to the signal pathway passage and transmittance decreases. This reduction is tangible in the low wavelengths under 320 nm. Besides a downward trend due to cut-off frequency over the transmission band, a redshift also occurs, arising from the manipulation and interference of the structure's electromagnetic modes. A drop of around 40 percent occurs under the semi-cylindrical demyelination in the modeled architecture, as can be observed in Fig.5(g). Afterward, the model's configuration is manipulated via the variation of the solid angle θ demonstrated in Fig.5(c). The angle θ is changed from 45 to 75, 95, 180, and 360 degrees while fixing the length and thickness of demyelination to 1000nm and 112nm, respectively. It is clear that a change in the demyelination means the generated electromagnetic modes under the excitation signal lead to manipulation by altering the effective refractive index (modal index) of the structure, which can have a constructive or destructive impact on the outgoing photonic spectra. In context related to changing the angle θ, the simulated results in Fig.5(h) indicate that the outgoing spectra change when the solid angle θ is altered. The manipulation of $\theta = 75$ degrees has a constructive impact on the outgoing wave in the transmission band. Owing to the constructive modal interference, the resonant peak is almost equal to the peak of the output wave without a demyelinated state at this angle, as seen in Fig.5(h). Relying on the constructive or destructive behavior of the generated electromagnetic modes under variation of θ, the outgoing signal shifts are associated with amplification or attenuation in some parts of the considered range—for instance, the transmittance factor increase in the wavelengths over 300nm when $\theta = 95$ degrees, relative to the transmittance, without demyelination. Consequently, the generated electromagnetic modes' constructive or destructive role in the myelin layers causes redshifts on the considered transmission band.

To get more insight into neurophotonics, it is interesting to note that employing optical signals and Nero-optical modulation techniques allow access to the brain's tiny points and deep areas to create cell-level signaling. It may also facilitate the possibility of access to a single nerve cell. Compared to the electrical signals that influence the larger area in the brain, optical signals can impact the smaller regions of the deep brain. From an applicable perspective, the feasibility of optical signal transmission through the myelin layers of the

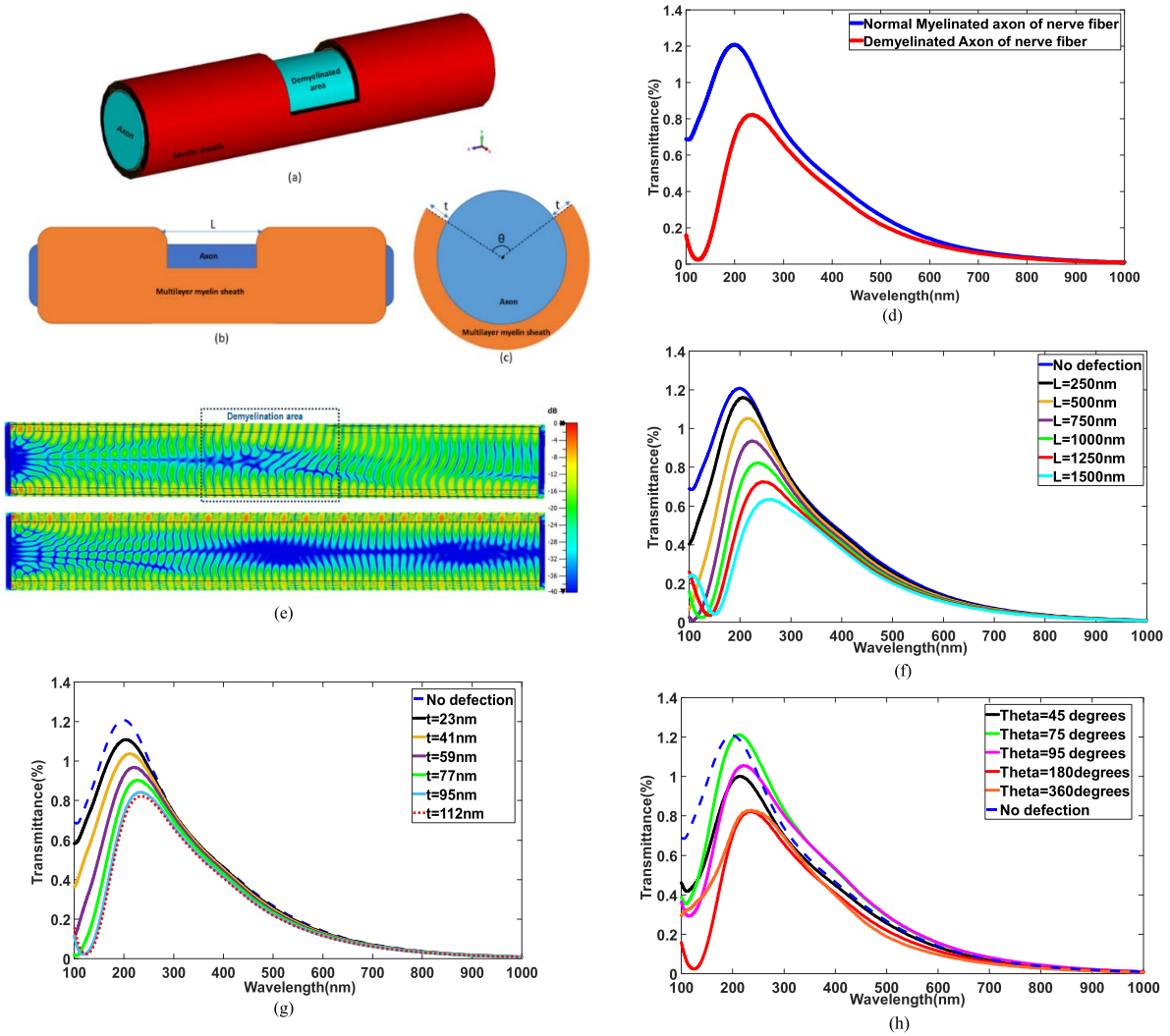

FIGURE 5. **(a) Schematic diagram of the demyelinated axon implemented in CST Microwave Studio, (b) the side view of the demyelinated nerve fiber, (c) the front view of the demyelinated nerve fiber, (d) Comparison of the transmittance calculated on the myelinated and demyelinated axon, (e) Electric field distribution across the myelinated axon model under stimulation of myelin layers at the transmittance's peaks (236.4nm for demyelinated axon and 199.08nm for myelinated axon) with myelin output (f) Variations of demyelinated axon's transmittance under demyelination's length change, (g) Variations of demyelinated axon's transmittance under demyelination's thickness change, (h) Variations of demyelinated axon's transmittance under demyelination's θ changes.**

nerve fiber and introducing it as a communication link for signaling can show the potential for deep brain stimulation and neuron-to-neuron communication that plays a vital role in the treatment plans of different mental diseases. Besides, evaluation of optical signal transmission spectra may provide the possibility for detection of demyelinating events in the nervous system, although absorption problems can be challenging. Further, the precise understanding of the functional mechanism of demyelination progression over the nerve fiber opens new horizons in diagnosis and treatment under the signal analysis arising from intracellular communications inside the brain and helps identify the neurons undertaking the risky status.

B. EFFECTIVE REFRACTIVE INDEX OF NERVE FIBER BASED ON STACKED MYELIN LAYERS

As mentioned above, the interference of electromagnetic modes in the nerve's configuration plays a decisive role in the conduction and transition of photons in the nerve [25], [26]. The simulated results indicate manipulating the nerve's geometrical configuration leads to modal interference during photon transmission in the myelinated axon, which can have a destructive or constructive impact on the outgoing signal in the neuronal communication system. The interference of the generated electromagnetic modes during light propagation within the nerve channel changes the effective refractive index of the structure, which implies a variation of output signal intensity and the shift of the spectral response transmission band. Hence, it is crucial to evaluate the myelinated axon's effective refractive index to depict the nerve's functioning under light stimulation and photon transmission. From an electrooptic viewpoint, the interaction between light and the multilayered structures has been analyzed by the transfer matrix method (TMM), in which reflectance is an important factor for various applications [49], [50]. Inspired by this nanoscale feature of nerve fibers, reflectance resulting

from modulation of light and the multilayered nerve fibers themselves has attracted particular attention to differentiate myelinated and unmyelinated axons [18]. In this section, our aim is to engineer the impact of demyelination on the reflectance parameter to achieve a precise understanding based on the established concepts of physics. Thus, the reflectance spectra of myelinated and demyelinated axons under an external light incidence are compared. First, the reflectance coefficient of the normal myelinated axon modeled in the previous section is obtained. Reflectance is the relationship between the amount of light is reflected (I_r) from the thin film nerve and the original amount of light (I_0) is incident, which is defined by [41]:

$$R_{(dB)} = 10.\log(\frac{I_r}{I_0}) \tag{2}$$

A gaussian excitation signal with a peak intensity of 1 v/m applied to the waveguide port in CST Microwave Studio's environment excites the configuration from the top. To be more precise, we choose a waveguide port as an excitation port located at the top side of the nerve model, and excitation wave is incident from the top perpendicularly toward the nerve structure, as illustrated in Fig.6(a).

Furthermore, due to massive meshing, high processing time, and the simulation's error probability during architecture's analysis because of modal distortion in the lower wavelengths of the transmission band, the simulation range is considered between 300nm to 1 μm. This shift aids in having a reliable analysis of the myelinated axon's performance while interacting with the incidence of the stimulation wave and achieving reflectance factor. Moreover, the main goal is to find the reflectance variation undergoing demyelination. For this, the reflectance of a normal myelinated axon is achieved, and then a demyelinated area with a length of 1000 nm and depth of 112 nm is created. Further, the length of demyelination is set at 500 nm and 1500 nm to assess the structure's optical behavior when the depth is the same as 112nm. The results demonstrated in Fig.6(b) express that demyelination can alter the spectral response's reflectance characteristic. An increase in L causes a gradual reduction in the reflected wave percentage, especially in wavelengths over 530nm. The reflectance amplitude as a primary indicator can distinguish a demyelinated axon from a myelinated one. More energy is absorbed by the demyelinated axon when the defection area expands due to the manipulation of the structure's effective refractive index. Also, the increase in L that this behavior may result in from phase mismatch of the myelin's layers leads to a saturation state. Next, the impact of the myelin sheath layers on the reflectance factor is evaluated. To do so, the depth of the demyelination area is changed to 23 nm, 77 nm, and 99 nm based on the main layered section of the myelin sheath depicted earlier. The spectra achieved from these variations indicate the tangible drop that occurs in the reflection band over 500 nm. The reflected electromagnetic components follow a declining trend that becomes saturated with an increase

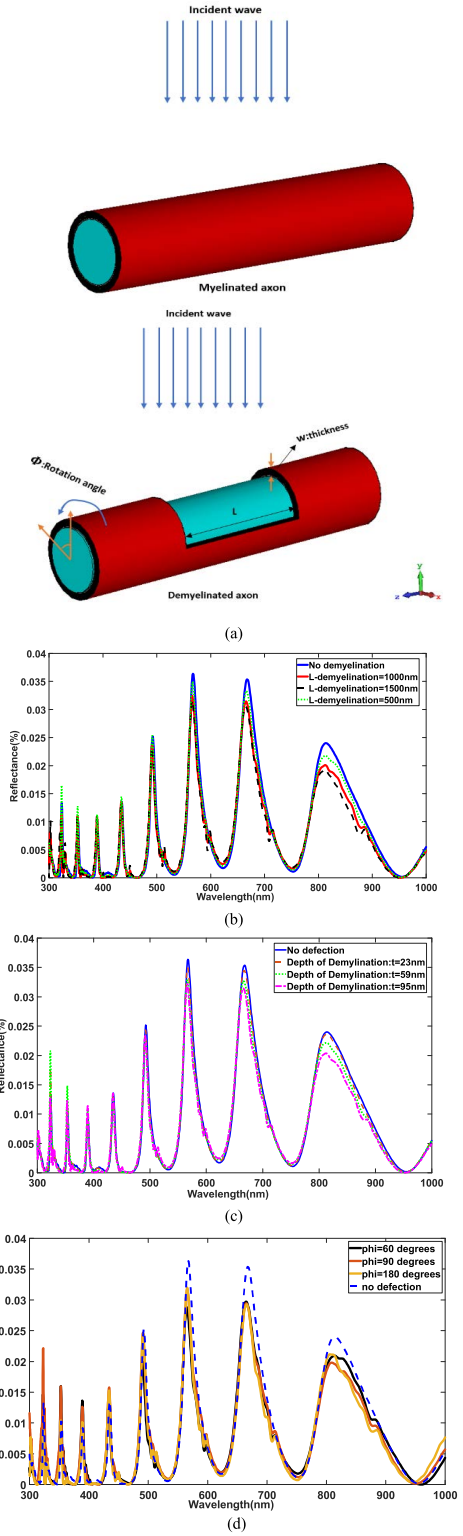

FIGURE 6. (a) Stimulation schematic of the myelinated and demyelinated axon by external light incidence, (b) the simulated reflectance spectra undertaking the increase in demyelination's length changes [L], (c) the simulated reflectance spectra undertaking the demyelination's depth variation [t], (d) the simulated reflectance spectra under demyelinated axon's rotation with the angle [φ].

in the depth of demyelination because of phase mismatching of the reflected field components. Interestingly, in lower

wavelengths, the spectral responses experience a significant rise in the reflection band, which results from the constructive effect of the propagating modes. As shown above, the incident vector is assumed to irradiate perpendicularly on the demyelination area. We further investigate the impact of incidence angle on the reflectance; thus, the suggested configuration is rotated as much as φ, set to 60, 90, and 180 degrees, as shown in Fig.6. Our objective is to understand the role of incidence direction on reflectance to detect the demyelination area. The reflectance parameter is varied by rotating the demyelinated nerve configuration. Changes in the incidence angles significantly alter the amplitude of reflectance in the wavelength range. Indeed, the rotation of nerve configuration, that is, angle variation of incidence, leads to manipulating the polarization of the reflected wave, which changes the reflectance. This manipulation can have constructive or destructive effects in the reflection band, as seen in Fig.6(d). As a practical point of view, it is significant to express; demyelination imaging in nanoscale and its analysis based on reflectometry technique can help diagnose earlier the disease before its development, which may facilitate the treatment process due to the small size of demyelination using the efficient drug plans, for example among Alzheimer's and MS patients. In other words, nanoscale demyelination detection and analysis can improve and accelerate the diagnosis process and treatment plan.

To efficiently implement the calculation mentioned above and understand the modal index's role under structural variations, we explore the effective refractive indexes resulting from the aforementioned changes. We employ an exact solution method to calculate the effective refractive index related to the nerve model, which is used for a slab structure [51], [52]. Based on this method, The effective refractive index of the nerve under the impact of manipulating demyelination size and changing the incidence angles are obtained. The achieved modal index in Fig.7 (a) illustrates the variations of the effective refractive index for the nerve model under demyelination length change on the considered spectral range. As observed, length variations create a tangible shift toward shorter wavelengths that function like a blueshift in the visible spectrum. Also, the effective refractive index value with a reduction drop of 0.05 at peak alters under the defined defection. The modal index's spectra also follow a diminishing trend relative to no defection state at the peak value in the NIR range.

To visualize better, the considered wavelength range is divided into sub-bands to demonstrate the effect of the different lengths of demyelination on the modal index, as seen in Fig.7 (b), (c), and (d). Afterward, the modal index of nerve configuration under thickness variation and structural rotation is calculated using the exact solution method, as shown in Fig.8 and Fig.9. The results in Fig.8 presents a significant blueshift in the modal index's spectra in the visible range due to increasing demyelination. For the sake of better understanding, when the light is incident on the demyelinated nerve, changes in the size of demyelination lead to the reflected spectra with the different phase velocities. Thus, various delays in phase constants of the reflected spectra create a form of blueshift on the reflection band.

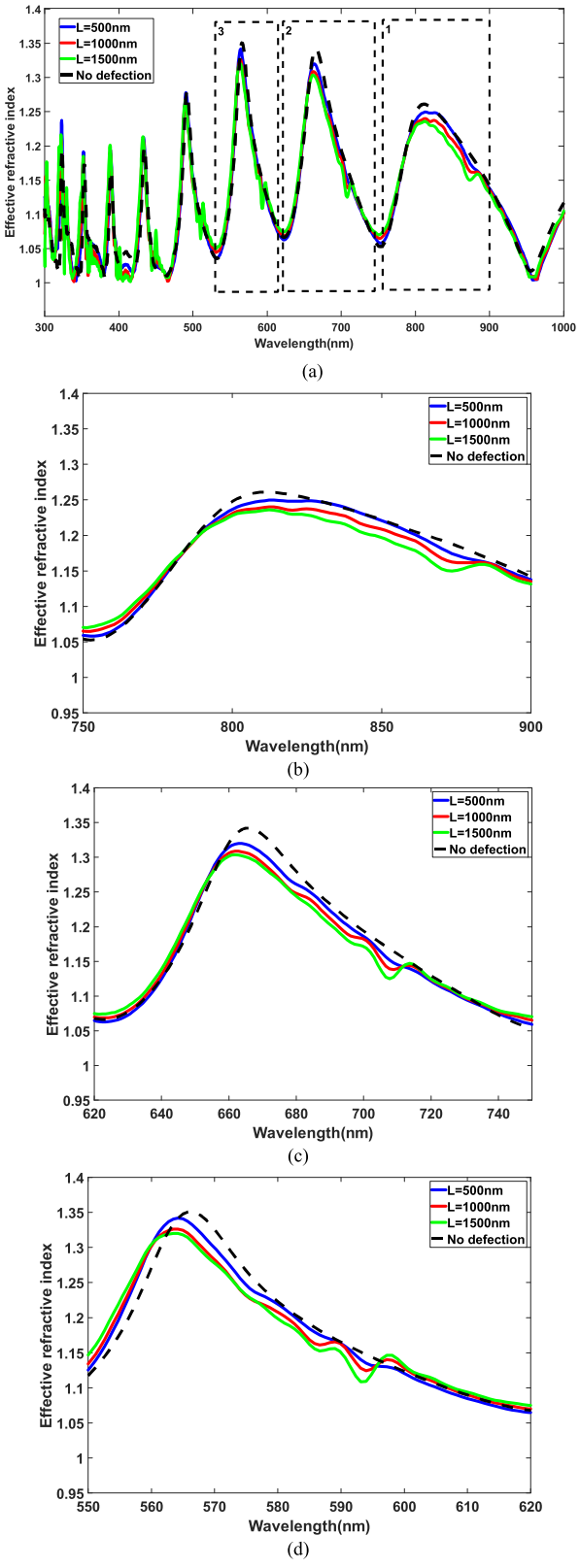

FIGURE 7. (a) The calculation of the effective refractive index (modal index) variation due to the demyelination's length changes with the sub-bands considered as follows (b) (750 nm -900 nm), (c) (620 nm -750 nm) and (d) (550 nm -620 nm).

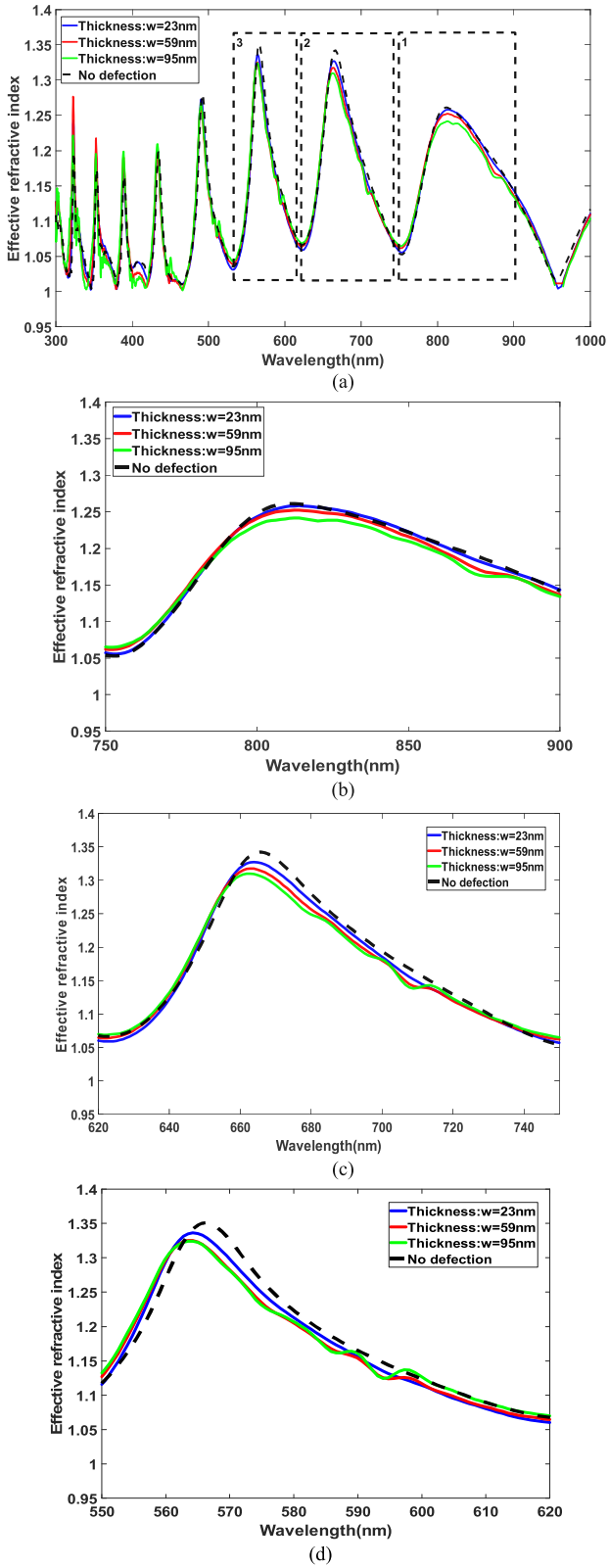

FIGURE 8. The calculation of the effective refractive index (modal index) variations due to the demyelination's thickness changes with the sub-band selected as follows: (b) (750 nm -900 nm), (c) (620 nm -750 nm), and (d) (550 nm-620 nm).

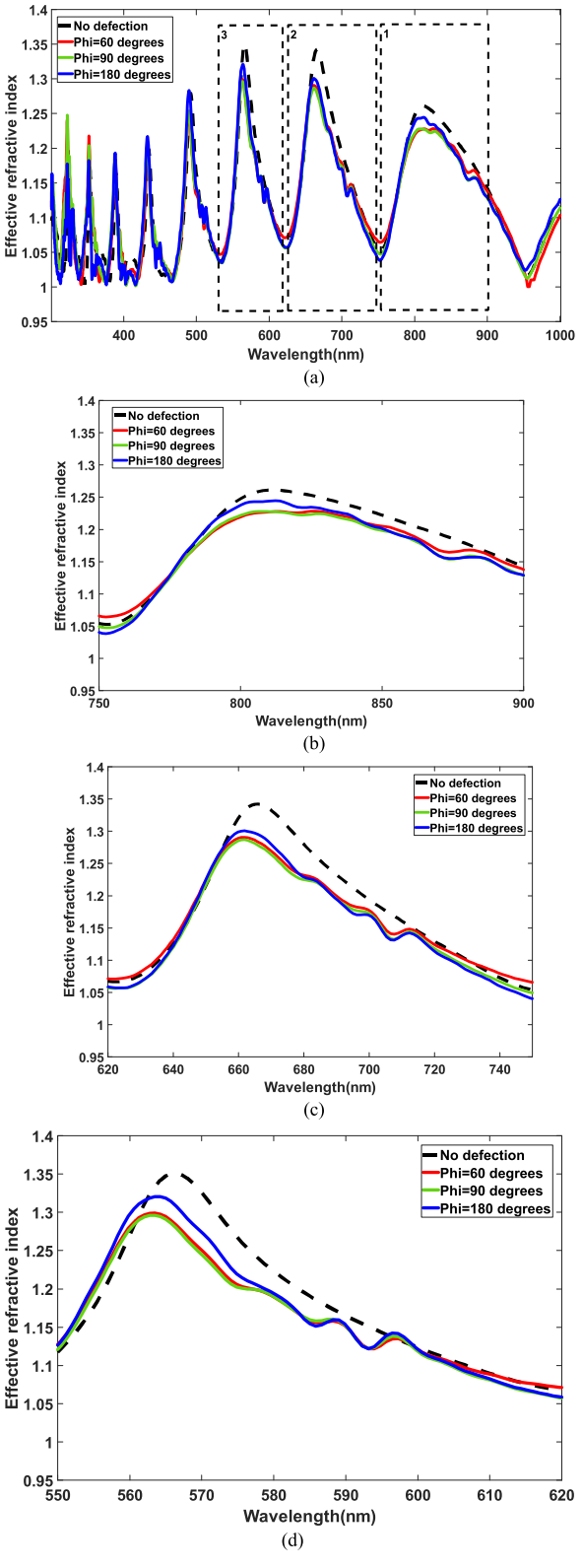

FIGURE 9. The calculation of the effective refractive index (modal index) variations due to the demyelination's demyelinated axon's rotation relative to light incidence direction (variation of φ) with the sub-band selected as follows: (b) (750 nm -900 nm), (c) (620 nm -750 nm) and (d) (550 nm-620 nm).

Similarly, the incidence angle of the excitation wave also changes the effective refractive index since the resultant of the reflected electromagnetic components alters under the influence of polarization variation, as shown in Fig.9. Therefore, a change in nerve configuration manipulates the equivalent modal index of nerve fiber that concludes the variation of propagation modes, thus shifting the spectral response of reflectance. This framework can provide a robust comparison between the myelinated axon and the demyelinated axon and present distinctions.

C. CHARACTERIZATION OF THE MYELINATED AXON BY GRAPHENE PHOTONIC STRUCTURE

Notably, neuronal communication is an electrochemical procedure in which nerve fibers function as communication channels to transmit signals between nerve cells. As already mentioned, the myelinated axon serves as a suitable platform to increase the efficiency of signal conduction [53]. In contrast, demyelination is introduced as the main cause of MS, whereby the myelin's layers are damaged, and the signaling between cells is obstructed. Hence, the detection and recognition of demyelinated axons based on spectral characterization is a potentially practical approach for early warning and prediction of treatment mechanisms. Herein, we propose a new technique for the detection and identification of nerve fibers, whether myelinated or demyelinated. We suggest this method based on the theory of refractive index sensing, which posits that the absorption of graphene structures is very sensitive to the different ambient refractive indexes [54]–[56].

Graphene is a powerful 2D-nanomaterial comprising carbon atoms in a monolayer arranged in a honey lattice from an optical point of view. In the optical range, the surface plasmon polariton properties of graphene also have the potential to provide sharp peaks in the broad region of wavelength spectra utilizing light incidence [57], [58]. In neuroscience applications, graphene-based materials are employed to distinguish nerve cells and axonal alignment using photoelectric properties. It has successfully highlighted that graphene can provide the potential for the distinction between non-neuronal and neuronal interfaces [59], [60]. On the ot$\mu\mu$her hand, it has been established that defections and impurities in structures constructed based on graphene materials alter these systems' electric and vibrational properties, which can be beneficial in facilitating the desired application [61]. Accordingly, we have a plan to develop a nanostructure based on the photonic structure to make a potential for the separation between demyelinated and myelinated axons. It is worth mentioning that the presence of graphene in the configuration of the photonic structure due to the sensitivity relative to mode index variations can play a determining role because defection of the nerve fiber model changes the effective refractive index, as indicated in the previous section.

For the sake of high biocompatibility, we choose a substrate of silicon dioxide (SiO2) with a thickness of 500 nm and dimensions 8μm $\times$ 8μm as the unit cell's substrate, a thin graphene sheet with a thickness of 10 nm covers the upper surface of the SiO2. The physical properties of graphene are considered as follows: the Fermi energy is set at 0.45ev, and the temperature and relaxation time is equal to 300K and 1ps, respectively. In addition, this kit is placed in Dulbecco's Modified Eagle Medium (DMEM) with an assumed refractive index of 1.345, which is suitable for cell culture [62]. The nerve configuration modeled as a sample is placed on the developed structure. Herein, we believe that this kit can function as a detection tool to indicate differentiation between myelinated or demyelinated axons using the reflected spectrum from the interaction between light and the kit. For this, we select a myelinated axon with the previous model and a defected axon with a demyelination length of 1000nm and a depth of 112nm, such as Fig.10(a) and (b). As expected, the simulated results in Fig.10 confirm that the reflectance spectrum presents some changes with the examination of the demyelinated axon. For further clarification, we divide the considered wavelength range into three sub-bands of the reflection band simulated, as seen in Fig.10 (c), (d), and (e).

By focusing on the visible-NIR, we observe a blueshift in the demyelinated axon's reflectance spectrum. The severe drop in the reflection band can be attributed to the plasmonic modes related to the graphene layer on the SiO2 substrate, in which the absorption factor is enhanced. From an electrooptic standpoint [63], light irradiation on the developed chip causes the stimulation of plasmonic modes of the graphene sheet derived from its complex refractive index, resulting in high peaks over the spectral response of absorbance, which indicates sharp falls in the reflectance spectrum. On the other hand, defection in the myelinated axon as demyelination accounts for the altered modal components of the reflected wave that may have a constructive or destructive impact on the reflectance. Hence, the defection of the myelin's layers can displace the reflectance response; in this case, a blueshift occurs. Besides, the constructive or destructive effect rooted in the phase matching or mismatching of the reflected field components can amplify or diminish in the reflectance spectrum of the demyelinated axon.

Based on graphene's plasmonic properties, we add an array of gold nanoparticles on top of the graphene sheet to enhance the plasmonic modes that play a crucial role in identifying myelinated axons. So, we employ an array of gold nanoparticles with a radius of 50 nm that is distributed on the surface of the graphene layer, as illustrated in Fig.11(a). This approach has the potential to modify the sensitivity of the developed chip [64]. As a theoretical analysis derived from the optoelectronic viewpoint to understand better, gold nanoparticles, compared to the other particles, have high stability and functionality in addition to biocompatibility. Due to their size and free electron density, interaction gold nanoparticles and graphene layer enhance localized surface plasmon resonance (LSPR) available in the structure. Therefore, it can be a proper choice to modify plasmonic modes over the reflection band undergoing optimal size [65], [66].

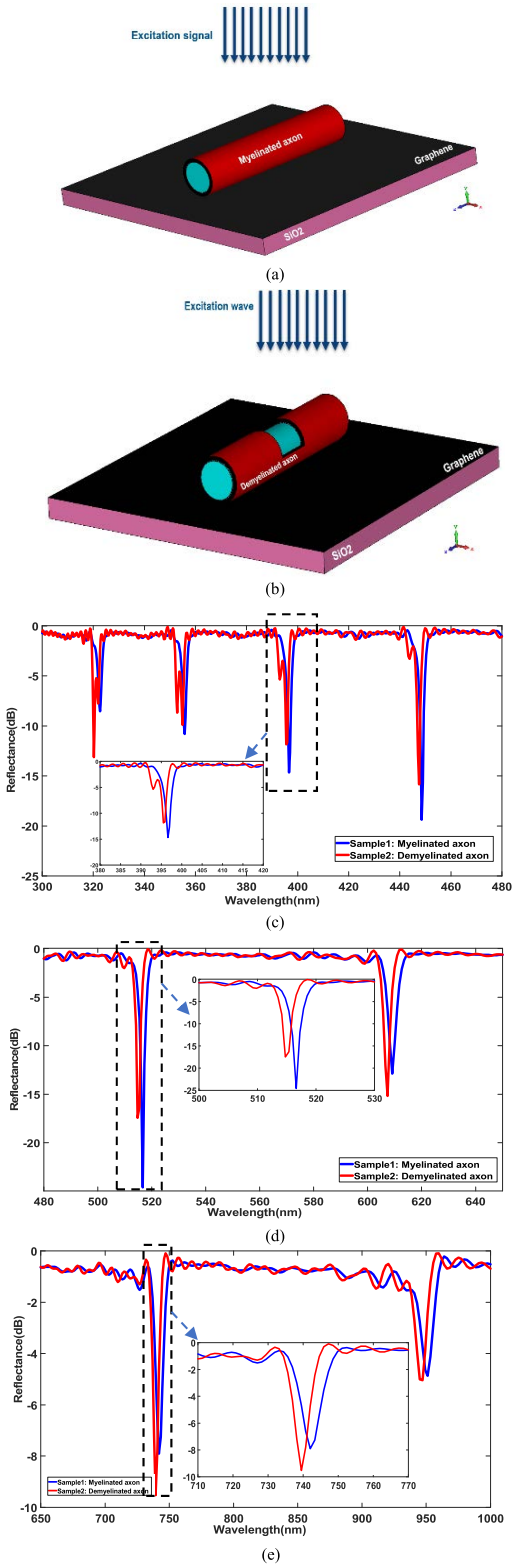

FIGURE 10. **(a) Spectroscopy plan for optical characterization of the myelinated axon by the designed biochip, (b) Spectroscopy schematic of the myelinated axon by the designed biochip, The contrast of reflectance spectra of myelinated and demyelinated axons in the wavelength window upon (c) 300nm-480nm, (d) 480nm-650nm and (e) 650nm-1μm.**

The nerve configuration is placed on the gold nanoparticles distributed over the graphene sheet. Similar to the previous process, the stimulation signal is incident on the structure from the top. For further precision, the desired spectral range (300 nm – 1 μm) is considered as three-wavelength windows: 300 nm - 480 nm, 480 nm – 650 nm, and 650 nm - 1 μm. The results in Fig.11 (b), (c), and (d) indicate that a blueshift occurs in reflectance spectra related to myelinated and demyelinated axons. In two of the wavelength windows (480 nm – 700 nm and 700 nm -1 μm) considered, it is clear that spectral response shifts under the impact of demyelination. The existence of gold nanoparticles on the graphene layer can provide greater bandwidth as well as amplification in the plasmonic mode compared to the prior structure. Fig.11 (e) shows the electric field distribution achieved on the biochip modified by gold nanoparticles at the wavelength of 679.7 nm, where the plasmonic effect of the nanoparticles is tangible.

To get a better insight into the results, the far-field radiation patterns of structures with myelinated and demyelinated axons on the biochip are calculated, as illustrated in Fig.11 (f) and (g); the distinction between them is well observed by contrasting the radiation pattern profiles. Besides, to indicate the impact of gold nanoparticles on the reflectance and the sensitivity of biochip, numerically, the lowest levels of the achieved reflectance on the reflection band in visible and NIR range are compared with each other as shown in Table. 1. As can be seen, the lowest value of reflectance in the visible range changes from -24.59dB to -31dB when a normal myelinated axon is placed on the substrate. Similarly, it changes from -17.6 dB to -25 dB while placing a demyelinated axon. For the NIR range, in the state of placing the normal myelinated axon and demyelinated axon, the variations mentioned above are from -7.9dB to -23dB and -9.52dB to -21dB, respectively. The presented results show that the sensitivity of biodevice changes considerably, especially in the NIR range with a significant improvement of more than -10dB, which can be a remarkable achievement in this practical range for neural imaging applications. These enhancements are due to constructive interference of plasmonic modes of gold nanoparticles and the graphene layer available in the configuration of the biochip.

Then, the effect of demyelination length and depth on the reflectance is determined using the modified biochip with gold nanoparticles shown in Fig12(a). First, the demyelination's length is altered from 1000nm to 500 nm and 1500 nm, while the depth is fixed at 112 nm. The simulated results show that the blueshift is a predominant phenomenon with the presence of demyelination. Focusing on the sharp points on the reflectance curve in Fig.12 (a) explains the significant shift toward the lower wavelengths under increasing demyelination length on the reflection band. Likewise, the simulated reflectance witnesses deeper declines under the impact of the increase in demyelination length (L). In other words, the increase in the length of defection on the nerve causes displacement in plasmonic modes, and amplification occurs in terms of absorption from phase matching, which results

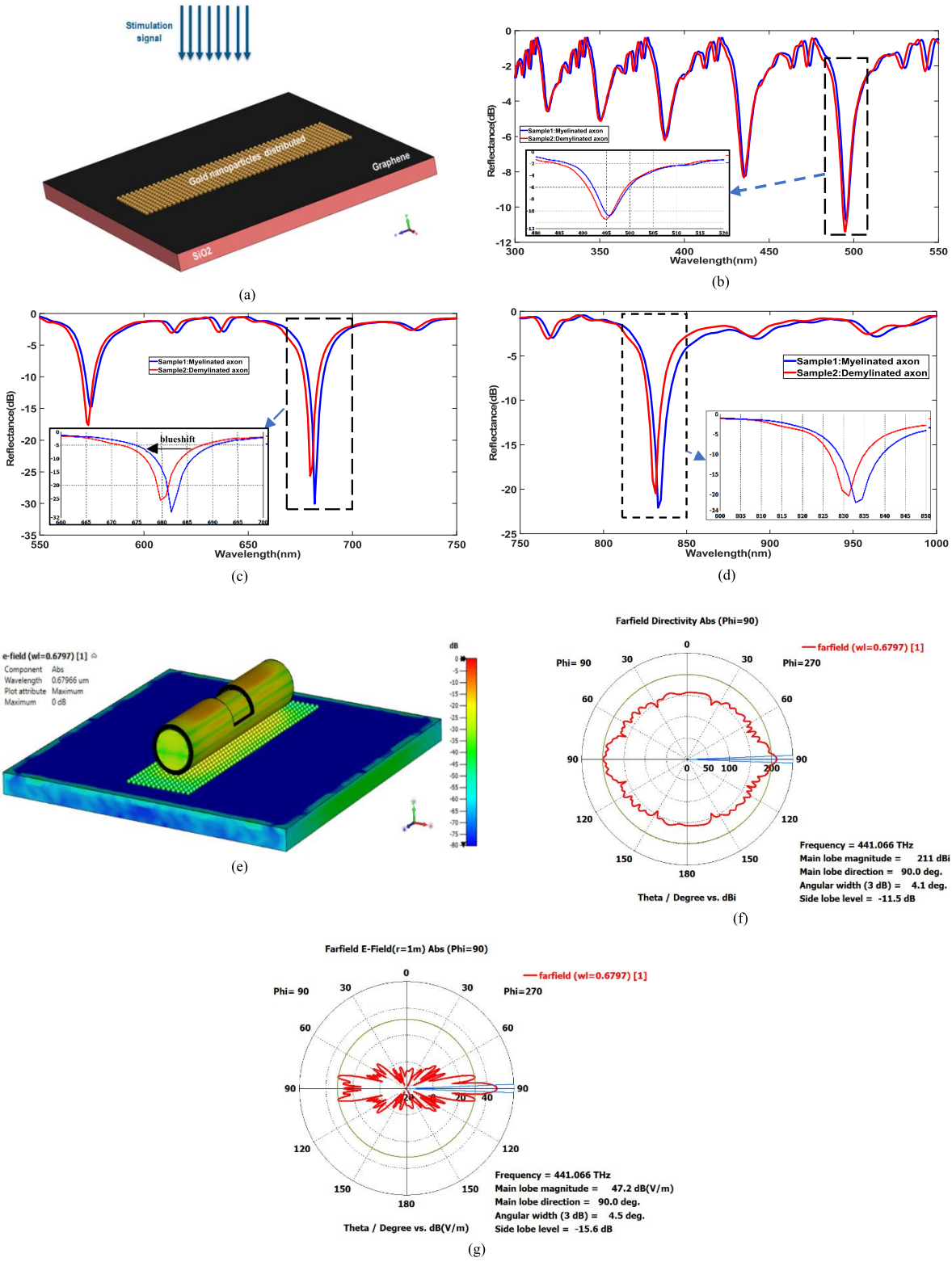

FIGURE 11. (a) The proposed biochip modified by gold nanoparticles, The contrast of reflectance spectra simulated of myelinated and demyelinated samples in the wavelength windows on (b) 300nm-550nm, (c) 550nm-750nm, and (d) 750nm-1μm, (e) Electric field distribution of the demyelinated axon placed on the biochip modified by gold nanoparticles at 679.7nm, (f) Polar radiation pattern of structure related to myelinated axon on the biochip at 679.7nm, (g) Polar radiation pattern of construction related to demyelinated axon on the biochip at 679.7nm.

TABLE 1. The lowest levels of reflectance (dB) on the spectral response of the developed biochip with or without gold nanoparticles (approximately).

Wavelength range(nm)	Without gold nanoparticles		With gold nanoparticles	
480-700	Myelinated axon	-24.59 dB	Myelinated axon	-31dB
	Demyelinated axon	-17.6 dB	Demyelinated axon	-25dB
700-1000	Myelinated axon	-7.9 dB	Myelinated axon	-23dB
	Demyelinated axon	-9.52 dB	Demyelinated axon	-21dB

in sharper minimal points of the reflection band. In addition, demyelination at depths of 23nm, 59nm, and 95nm could also be detected using the designed chip by contrasting the minimal points of reflectance spectra, as seen in Fig.12(b). In this state, we have assumed no change in the demyelination length of 1000nm. Indeed, the proposed structure for testing nerve samples is very sensitive to modal index variations resulting from physical damage to the nerve. After studying demyelination, we are then intended to focus on axon defection. In this regard, the middle of the axon in the modeled neve configuration is damaged by a gap, and the refractive index of the defection gap is equal to 1. The length of the axon's defection gap is set to 500nm, 1000nm, and 1500nm without any demyelination, as seen in Fig.13(a). We aim to understand whether the developed structure can detect axon damage by recognizing a change in the refractive index. The simulated results in Fig.13(b) indicate that the reflectance spectrum in the greater gap of axon damage experiences a deep fall. As a result, we can claim that the developed biochip can detect reflectance variations with the demyelination and damage to axons. As a practical point, the designed microchip can function as a unit cell and be placed in a periodic structure that gives this potential to evaluate macro-level samples.

Based on numerical simulations, it is demonstrated that spectral reflectometry and transmitometry can reveal and characterize the demyelinated axon in neuronal tissues. From a practical standpoint, imaging and monitoring the tiny tissues with high resolution in the brain can help the control of diseases development using drug plans. For instance, in MS patients, the possibility of access to nanoscope imaging of demyelinated axons, contrasting the achieved images, and monitoring the demyelination progression can have an impressive impact in terms of diagnosis and treatment plans and prevent the disease recurrence. In this regard, neural electronic devices such as the proposed neurophotonic pin as supplementary devices can improve the precision of neural sensing and imaging to obtain the images with an acceptable resolution. In addition, the designed nanochip can be used to estimate the demyelinated area's size using the established concepts based on diffraction theory and image processing mechanisms. Also, the proposed biochip has the potential to be applied for the detection of different failures of neural and heart signals due to the existence of the graphene layer that is very sensitive to physical changes.

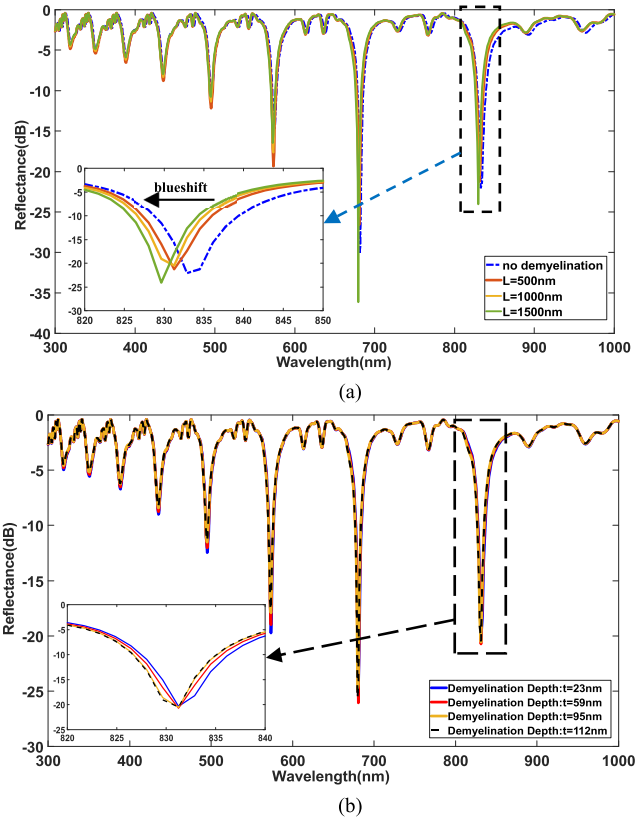

FIGURE 12. Spectral characterization of myelinated and demyelinated axons' reflectance under (a) demyelination's length variation, (b) demyelination's depth variation.

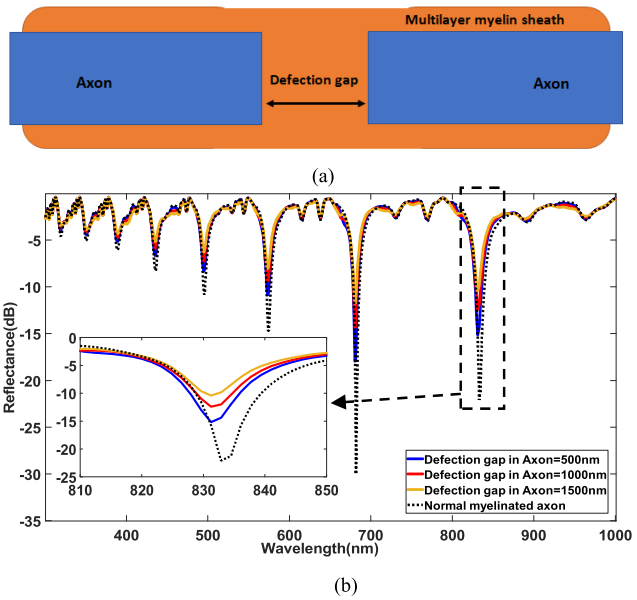

FIGURE 13. (a) A schematic diagram of defected axon in the myelinated axon (b) The contrast of reflectance spectra simulated from a nerve fiber with defected axon under different defection gap.

IV. CONCLUSION

This work outlined a new modality of plasmonic neurophotonics and spectral characterization for myelinated axons

with nanoscale demyelination. As a preliminary achievement, this study promotes a promising approach for differentiation between demyelinated and myelinated axons. Our findings indicated that the outgoing photonic signal spectrum experiences a resonance mode during the propagation across the myelin's layers, manipulated by demyelination. It is found that resonance occurred in the transmission band due to modeled thin-film structure of the myelinated axon with myelin's layers stacked that functions like a multilayer dielectric waveguide in the optical range, plays an essential role in more energy transfer towards the output. Besides, transmittance spectra witnessed a redshift under demyelination's size variation during the conduction of the photonic signal associated with a 40 percent drop as an example and the downward trend due to becoming close to the cut-off frequency of nerve channels.

Using the reflectance spectra under an external light incidence and comparing the simulated results, the demyelination effect on the nerve is extracted. The results reveal a blueshift in the nerve's reflectance spectra under the impact of demyelination size variations. Also, the demyelination effect on the effective refractive index is obtained through an exact analytical solution and indicated shifting waveguide modes of the myelinated axon by manipulating demyelination size. Motivated by these, we develop a graphene-based photonic structure as a biochip to identify demyelinated axons. The simulated results denote that the designed neurophotonic chip has the potential to detect demyelination's structural variations in the nerve fiber and characterize the damaged axons. We utilize gold nanoparticles to modify the biochip's sensitivity relative to the change of the modal index due to demyelination, more than -10 dB in NIR, as indicated in Table. 1. The framework employed for the proposed biochip design can provide a new approach for the fabrication of neurophotonic pins to facilitate neuronal imaging for deep brain applications.

AUTHOR CONTRIBUTION

In this work, Amir Maghoul designed the concept, did simulations, and wrote and revised the paper. Ilangko Balasingham technically and scientifically supervised the work, investigated and edited the paper, and reviewed and revised it. Ali Rostami also technically and scientifically advised and investigated and reviewed, and revised the work. Mladen Veletic technically contributed to writing the paper and revised and reviewed the work. Bige Deniz Unluturk revised and reviewed the article. Nilojan Gnanakulasekaran had a final check technically and edited it. All authors have read and agreed to the published version of the manuscript.

REFERENCES

[1] D. M. Lovinger, "Communication networks in the brain: Neurons, receptors, neurotransmitters, and alcohol," (in English), *Alcohol Res Health*, vol. 31, no. 3, pp. 196–214, 2008. [Online]. Available: https://pubmed.ncbi.nlm.nih.gov/23584863

[2] M. Bear, B. Connors, and M. A. Paradiso, *Neuroscience: Exploring the Brain*. Burlington, MA, USA: Jones & Bartlett, 2020.

[3] S. Herculano-Houzel, "The human brain in numbers: A linearly scaled-up primate brain," *Frontiers Hum. Neurosci.*, vol. 3, p. 31, Nov. 2009.

[4] A. Longstaff, *Neuroscience*. New York, NY, USA: Garland Science, 2011.

[5] J. E. Rinholm and L. H. Bergersen, "The wrap that feeds neurons," *Nature*, vol. 487, no. 7408, pp. 435–436, Jul. 2012, doi: 10.1038/487435a.

[6] D. K. Hartline and D. R. Colman, "Rapid conduction and the evolution of giant axons and myelinated fibers," *Current Biol.*, vol. 17, no. 1, pp. R29–R35, Jan. 2007.

[7] I. L. Arancibia-Cárcamo, M. C. Ford, L. Cossell, K. Ishida, K. Tohyama, and D. Attwell, "Node of Ranvier length as a potential regulator of myelinated axon conduction speed," *eLife*, vol. 6, p. e23329, Jan. 2017.

[8] K.-A. Nave, "Myelination and support of axonal integrity by glia," *Nature*, vol. 468, no. 7321, pp. 244–252, Nov. 2010.

[9] R. A. Rhoades and D. R. Bell, *Medical Physiology: Principles for Clinical Medicine*. Philadelphia, PA, USA: Williams & Wilkins, 2012.

[10] R. D. Fields, "Myelin—More than insulation," *Science*, vol. 344, no. 6181, pp. 264–266, Apr. 2014.

[11] G. F. Striedter, *Neurobiology: A Functional Approach*. Oxford, U.K.: Oxford Univ. Press, 2016.

[12] M. C. Ford, O. Alexandrova, L. Cossell, A. Stange-Marten, J. Sinclair, C. Kopp-Scheinpflug, M. Pecka, D. Attwell, and B. Grothe, "Tuning of Ranvier node and internode properties in myelinated axons to adjust action potential timing," *Nature Commun.*, vol. 6, no. 1, p. 8073, Nov. 2015, doi: 10.1038/ncomms9073.

[13] M. E. Bechler and C. French-Constant, "A new wrap for neuronal activity?" *Science*, vol. 344, no. 6183, pp. 480–481, May 2014.

[14] I. A. McKenzie, D. Ohayon, H. Li, J. P. de Faria, B. Emery, K. Tohyama, and W. D. Richardson, "Motor skill learning requires active central myelination," *Science*, vol. 346, no. 6207, pp. 318–322, Oct. 2014.

[15] M. Podbielska, N. Banik, E. Kurowska, and E. Hogan, "Myelin recovery in multiple sclerosis: The challenge of remyelination," *Brain Sci.*, vol. 3, no. 4, pp. 1282–1324, Aug. 2013. [Online]. Available: https://www.mdpi.com/2076-3425/3/3/1282

[16] M. M. Mehndiratta and N. S. Gulati, "Central and peripheral demyelination," (in English), *J. Neurosci. Rural Pract*, vol. 5, no. 1, pp. 84–86, 2014, doi: 10.4103/0976-3147.127887.

[17] K. Kamil, M. D. Yazid, R. B. H. Idrus, S. Das, and J. Kumar, "Peripheral demyelinating diseases: From biology to translational medicine," (in English), *Frontiers Neurol.*, vol. 10, p. 87, Mar. 2019, doi: 10.3389/fneur.2019.00087.

[18] J. Kwon, M. Kim, H. Park, B.-M. Kang, Y. Jo, J.-H. Kim, O. James, S.-H. Yun, S.-G. Kim, M. Suh, and M. Choi, "Label-free nanoscale optical metrology on myelinated axons *in vivo*," *Nature Commun.*, vol. 8, no. 1, p. 1832, Dec. 2017, doi: 10.1038/s41467-017-01979-2.

[19] Z. Xiang, C. Tang, C. Chang, and G. Liu, "A primary model of THz and far-infrared signal generation and conduction in neuron systems based on the hypothesis of the ordered phase of water molecules on the neuron surface I: Signal characteristics," *Sci. Bull.*, vol. 65, no. 4, pp. 308–317, Feb. 2020.

[20] Y. Liu, K. Wu, C. Liu, G. Cui, C. Chang, and G. Liu, "Amplification of terahertz/infrared field at the nodes of Ranvier for myelinated nerve," *Sci. China Phys., Mech. Astron.*, vol. 63, no. 7, Jul. 2020, Art. no. 274211, doi: 10.1007/s11433-019-1530-2.

[21] C. Lee, A. Lavoie, J. Liu, S. X. Chen, and B.-H. Liu, "Light up the brain: The application of optogenetics in cell-type specific dissection of mouse brain circuits," *Frontiers Neural Circuits*, vol. 14, p. 18, Apr. 2020, doi: 10.3389/fncir.2020.00018.

[22] S. Chen, J. Wu, A. Cai, N. Gonzalez, and R. Yin, "Towards minimally invasive deep brain stimulation and imaging: A near-infrared upconversion approach," *Neurosci. Res.*, vol. 152, pp. 59–65, Mar. 2020, doi: 10.1016/j.neures.2020.01.005.

[23] S. Chen, A. Z. Weitemier, X. Zeng, L. He, X. Wang, Y. Tao, A. J. Y. Huang, Y. Hashimotodani, M. Kano, H. Iwasaki, and L. K. Parajuli, "Near-infrared deep brain stimulation via upconversion nanoparticle-mediated optogenetics," *Science*, vol. 359, no. 6376, pp. 679–684, 2018.

[24] A. Zangari, D. Micheli, R. Galeazzi, A. Tozzi, V. Balzano, G. Bellavia, and M. E. Caristo, "Photons detected in the active nerve by photographic technique," *Sci. Rep.*, vol. 11, no. 1, p. 3022, Dec. 2021, doi: 10.1038/s41598-021-82622-5.

[25] S. Kumar, K. Boone, and J. Tuszyński, P. Barclay, and C. Simon, "Possible existence of optical communication channels in the brain," *Sci. Rep.*, vol. 6, p. 36508, Nov. 2016, doi: 10.1038/srep36508.

[26] A. Maghoul, A. Khaleghi, and I. Balasingham, "Engineering photonic transmission inside brain nerve fibers," *IEEE Access*, vol. 9, pp. 35399–35410, 2021, doi: 10.1109/ACCESS.2021.3062299.

[27] G. Liu, C. Chang, Z. Qiao, K. Wu, Z. Zhu, G. Cui, W. Peng, Y. Tang, J. Li, and C. Fan, "Myelin sheath as a dielectric waveguide for signal propagation in the mid-infrared to terahertz spectral range," *Adv. Funct. Mater.*, vol. 29, no. 7, Feb. 2019, Art. no. 1807862, doi: 10.1002/adfm.201807862.

[28] M. Menzel, M. Axer, H. De Raedt, I. Costantini, L. Silvestri, F. S. Pavone, K. Amunts, and K. Michielsen, "Toward a high-resolution reconstruction of 3D nerve fiber architectures and crossings in the brain using light scattering measurements and finite-difference time-domain simulations," *Phys. Rev. X*, vol. 10, no. 2, Apr. 2020, Art. no. 021002.

[29] P. P. Sordillo and L. A. Sordillo, "The mystery of chemotherapy brain: Kynurenines, tubulin and biophoton release," *Anticancer Res.*, vol. 40, no. 3, pp. 1189–1200, Mar. 2020, doi: 10.21873/anticanres.14061.

[30] R. Tang and J. Dai, "Biophoton signal transmission and processing in the brain," *J. Photochem. Photobiol. B, Biol.*, vol. 139, pp. 71–75, Oct. 2014, doi: 10.1016/j.jphotobiol.2013.12.008.

[31] K. Susuki, "Myelin: A specialized membrane for cell communication," *Nature Educ.*, vol. 3, no. 9, p. 59, 2010.

[32] Y. Poitelon, A. M. Kopec, and S. Belin, "Myelin fat facts: An overview of lipids and fatty acid metabolism," *Cells*, vol. 9, no. 4, p. 812, Mar. 2020.

[33] W. A. Catterall, I. M. Raman, H. P. C. Robinson, T. J. Sejnowski, and O. Paulsen, "The hodgkin-huxley heritage: From channels to circuits," *J. Neurosci.*, vol. 32, no. 41, pp. 14064–14073, Oct. 2012, doi: 10.1523/jneurosci.3403-12.2012.

[34] E. M. Gibson, D. Purger, C. W. Mount, A. K. Goldstein, G. L. Lin, L. S. Wood, I. Inema, S. E. Miller, G. Bieri, J. B. Zuchero, B. A. Barres, P. J. Woo, H. Vogel, and M. Monje, "Neuronal activity promotes oligodendrogenesis and adaptive myelination in the mammalian brain," *Science*, vol. 344, no. 6183, May 2014, Art. no. 1252304, doi: 10.1126/science.1252304.

[35] T. M. Merklein, "High resolution measurement of multilayer structures," *Appl. Opt.*, vol. 29, no. 4, pp. 505–511, 1990, doi: 10.1364/AO.29.000505.

[36] A. J. Schain, R. A. Hill, and J. Grutzendler, "Label-free *in vivo* imaging of myelinated axons in health and disease with spectral confocal reflectance microscopy," *Nature Med.*, vol. 20, no. 4, pp. 443–449, Apr. 2014, doi: 10.1038/nm.3495.

[37] Y.-S. Ku, K. C. Huang, and W. Hsu, "Characterization of high density through silicon vias with spectral reflectometry," *Opt. Exp.*, vol. 19, no. 7, pp. 5993–6006, 2011, doi: 10.1364/OE.19.005993.

[38] J. Kwon and M. Choi, "Spectral reflectometric microscopy on myelinated axons *in situ*," *JoVE*, vol. 137, p. e57965, Jul. 2018.

[39] E. Rahman, M. B. Powner, P. A. Kyriacou, and I. F. Triantis, "Assessment of the complex refractive indices of Xenopus laevis sciatic nerve for the optimization of optical (NIR) neurostimulation," *IEEE Trans. Neural Syst. Rehabil. Eng.*, vol. 26, no. 12, pp. 2306–2314, Dec. 2018, doi: 10.1109/TNSRE.2018.2878107.

[40] Y. Fukui, S. Hayasaka, K. S. Bedi, H. S. Ozaki, and Y. Takeuchi, "Quantitative study of the development of the optic nerve in rats reared in the dark during early postnatal life," (in English), *J. Anatomy*, vol. 174, pp. 37–47, 1991. [Online]. Available: https://pubmed.ncbi.nlm.nih.gov/2032941 https://www.ncbi.nlm.nih.gov/pmc/articles/PMC1256041/.

[41] M. T. Sebastian, R. Ubic, and H. Jantunen, *Microwave Materials and Applications*. Hoboken, NJ, USA: Wiley, 2017.

[42] D. M. Shyroki and A. V. Lavrinenko, "Dielectric multilayer waveguides for TE and TM mode matching," *J. Opt. A, Pure Appl. Opt.*, vol. 5, no. 3, p. 192, 2003.

[43] Y. Mitelman and E. Malov, "Mathematical model for analysis of multilayered circular waveguides," in *Proc. 2nd Int. Conf. Ind. Eng., Appl. Manuf. (ICIEAM)*, May 2016, pp. 1–4, doi: 10.1109/ICIEAM.2016.7911602.

[44] A. Eriksson, L. Beilina, and T. M. Larsen, "Reconstruction of annular bi-layered media in cylindrical waveguide section," *J. Math. Ind.*, vol. 7, no. 1, p. 6, Dec. 2017, doi: 10.1186/s13362-017-0036-x.

[45] G. P. Agrawal, *Fiber-Optic Communication Systems*. Hoboken, NJ, USA: Wiley, 2012.

[46] I. Wilson, C. Vitelli, G. K. Yu, G. Pacheco, J. Vincelette, S. Bunting, and S. Sisó, "Quantitative assessment of neuroinflammation, myelinogenesis, demyelination, and nerve fiber regeneration in immunostained sciatic nerves from twitcher mice with a tissue image analysis platform," *Toxicol. Pathol.*, vol. 49, no. 4, pp. 950–962, Jun. 2021, doi: 10.1177/0192623321991469.

[47] J. G. Lyon, L. Karumbaiah, and R. V. Bellamkonda, "Neural tissue engineering," in *Neural Engineering*, B. He, Ed., Cham, Switzerland: Springer, 2020, pp. 639–667.

[48] E. Bélanger, F. P. Henry, R. Vallée, M. A. Randolph, I. E. Kochevar, J. M. Winograd, C. P. Lin, and D. Côté, "*In vivo* evaluation of demyelination and remyelination in a nerve crush injury model," *Biomed. Opt. Exp.*, vol. 2, no. 9, pp. 2698–2708, 2011, doi: 10.1364/BOE.2.002698.

[49] T. G. Nguyen and A. Mitchell, "Analysis of optical waveguides with multilayer dielectric coatings using plane wave expansion," *J. Lightw. Technol.*, vol. 24, no. 1, pp. 635–642, Jan. 2006, doi: 10.1109/JLT.2005.860158.

[50] O. Matsuda and O. B. Wright, "Reflection and transmission of light in multilayers perturbed by picosecond strain pulse propagation," *J. Opt. Soc. Amer. B, Opt. Phys.*, vol. 19, no. 12, pp. 3028–3041, 2002, doi: 10.1364/JOSAB.19.003028.

[51] S. Y. El-Zaiat, "Determination of the complex refractive index of a thick slab material from its spectral reflectance and transmittance at normal incidence," *Optik*, vol. 124, no. 2, pp. 157–161, Jan. 2013.

[52] E. Nichelatti, "Complex refractive index of a slab from reflectance and transmittance: Analytical solution," *J. Opt. A, Pure Appl. Opt.*, vol. 4, no. 4, pp. 400–403, Jul. 2002.

[53] D. B. Unal, S. R. Caliari, and K. J. Lampe, "Engineering biomaterial microenvironments to promote myelination in the central nervous system," *Brain Res. Bull.*, vol. 152, pp. 159–174, Oct. 2019, doi: 10.1016/j.brainresbull.2019.07.013.

[54] L. Sun, Y. Zhang, C. Zhang, Y. Dai, Z. Xin, S. Zhu, X. Yuan, C. Min, and Y. Yang, "Refractive index sensing and imaging based on polarization-sensitive graphene," *Opt. Exp.*, vol. 27, no. 20, pp. 29273–29286, 2019, doi: 10.1364/OE.27.029273.

[55] F. Xing, Z.-B. Liu, Z.-C. Deng, X.-T. Kong, X.-Q. Yan, X.-D. Chen, Q. Ye, C.-P. Zhang, Y.-S. Chen, and J.-G. Tian, "Sensitive real-time monitoring of refractive indexes using a novel graphene-based optical sensor," *Sci. Rep.*, vol. 2, p. 908, Nov. 2012, doi: 10.1038/srep00908.

[56] Q. Ye, J. Wang, Z. Liu, Z.-C. Deng, X.-T. Kong, F. Xing, X.-D. Chen, W.-Y. Zhou, C.-P. Zhang, and J.-G. Tian, "Polarization-dependent optical absorption of graphene under total internal reflection," *Appl. Phys. Lett.*, vol. 102, no. 2, Jan. 2013, Art. no. 021912.

[57] A. K. Geim and K. S. Novoselov, "The rise of graphene," *Nature Mater.*, vol. 6, no. 3, pp. 183–191, 2007, doi: 10.1038/nmat1849.

[58] K. S. Novoselov, A. K. Geim, S. V. Morozov, D. Jiang, Y. Zhang, S. V. Dubonos, I. V. Grigorieva, and A. A. Firsov, "Electric field effect in atomically thin carbon films," *Science*, vol. 306, no. 5696, pp. 666–669, 2004.

[59] S. K. Rastogi, G. Raghavan, G. Yang, and T. Cohen-Karni, "Effect of graphene on nonneuronal and neuronal cell viability and stress," *Nano Lett.*, vol. 17, no. 5, pp. 3297–3301, May 2017, doi: 10.1021/acs.nanolett.7b01215.

[60] A. Solanki, S.-T.-D. Chueng, P. T. Yin, R. Kappera, M. Chhowalla, and K.-B. Lee, "Axonal alignment and enhanced neuronal differentiation of neural stem cells on graphene-nanoparticle hybrid structures," *Adv. Mater.*, vol. 25, no. 38, pp. 5477–5482, Oct. 2013.

[61] P. T. Araujo, M. Terrones, and M. S. Dresselhaus, "Defects and impurities in graphene-like materials," *Mater. Today*, vol. 15, no. 3, pp. 98–109, 2012, doi: 10.1016/S1369-7021(12)70045-7.

[62] E. Kim, K. Ehrmann, S. Uhlhorn, D. Borja, E. Arrieta-Quintero, and J.-M. Parel, "Semiautomated analysis of optical coherence tomography crystalline lens images under simulated accommodation," *J. Biomed. Opt.*, vol. 16, no. 5, 2011, Art. no. 056003, doi: 10.1117/1.3574613.

[63] F. Jabbarzadeh, M. Heydari, and A. Habibzadeh-Sharif, "A comparative analysis of the accuracy of kubo formulations for graphene plasmonics," *Mater. Res. Exp.*, vol. 6, no. 8, May 2019, Art. no. 086209.

[64] J. Bao, N. Hashemi, J. Guo, and N. N. Hashemi, "Effects of graphene layer and gold nanoparticles on sensitivity of humidity sensors," *J. Micromanufacturing*, vol. 3, no. 1, pp. 20–27, May 2020, doi: 10.1177/2516598419896130.

[65] Z. Osváth, A. Deák, K. Kertész, G. Molnár, G. Vértesy, D. Zámbó, C. Hwang, and L. P. Biró, "The structure and properties of graphene on gold nanoparticles," *Nanoscale*, vol. 7, no. 12, pp. 5503–5509, 2015, doi: 10.1039/C5NR00268K.

[66] J.-H. Lee, H.-Y. Cho, H. Choi, J.-Y. Lee, and J.-W. Choi, "Application of gold nanoparticle to plasmonic biosensors," *Int. J. Mol. Sci.*, vol. 19, no. 7, p. 2021, Jul. 2018. [Online]. Available: https://www.mdpi.com/1422-0067/19/7/2021.

AMIR MAGHOUL received the B.S. and M.S. degrees in electrical engineering, in 2006 and 2009, respectively, and the Ph.D. degree in electrical engineering-optical integrated circuits from the University of Tabriz, Iran, in 2017. During the Ph.D. level, he focused on nanoantennas design, nonlinear properties of nanoantennas, and simulation of computational nanophotonic structures. In 2017, he joined Islamic Azad University (IAU) as an Assistant Professor and was occupied with teaching different courses at bachelor's and master's levels. From 2017 to 2019, he continued his collaboration with the Photonic and Crystal Laboratory, University of Tabriz, and ASEPE Company in nanophotonic field. He is currently doing his research as a Postdoctoral Fellowship with the Norwegian University of Science and Technology (NTNU), Norway. His research interests include micro/nanoantenna design for optical and medical applications, computational neuroscience, and simulating in nanophotonic structures.

ALI ROSTAMI received the Ph.D. degree in photonic/electronic engineering from the Amirkabir University of Technology, Tehran, Iran, in 1998. He was on sabbatical leave with the University of Toronto and the University of California, from 2004 to 2005, the Photonic Group and the Electrical Engineering Department, in 2014, respectively. He was selected as a Distinguished Researcher with the University of Tabriz several times. In 2006 and 2010, he was elected as a Distinguished Researcher in the engineering field in Iran. Also, he was elected as a Best Professor in Iran, in 2011. He is currently a Full Professor in electronic engineering and photonics science with the University of Tabriz. He is also the Founder of the Photonics and Nanocrystals Research Laboratory (PNRL), University of Tabriz. The School of Engineering-Emerging Technologies is another project that he established with the University of Tabriz, in 2008. He is the author and coauthor of more than 380 scientific international journals and more than 500 conference papers and 25 textbooks in Persian, 25 book chapters, more than 15 patents, and five books in the English language. Also, he collaborates with some international journals on their reviewer board and works on the editorial committee of two Iranian journals and five international journals. His research interests include optical integrated circuits and optoelectronic devices and quantum communication, computing, and processing. He is a member of the Optical Society of America. Besides, he has been the Chair of the Center of Excellence for Mechatronics for two years, since 2005. Also, he is an Associate Editor of *Journal of Nanotechnology* Frontiers and *Nanoelectronics* Section. He has served on several other committees and panels in government and industry and at technical conferences.

MLADEN VELETIĆ received the B.Sc. and M.Sc. degrees in electronics and telecommunications from the Faculty of Electrical Engineering, University of Banja Luka (UNIBL), Bosnia and Herzegovina, in 2010 and 2012, respectively, and the joint Ph.D. degree in telecommunications from the Department of Electronic Systems, Norwegian University of Science and Technology (NTNU), Norway, and the Faculty of Electrical Engineering, UNIBL. From 2011 to 2017, he worked as a Senior Teaching and a Research Assistant with UNIBL. He is currently a Postdoctoral Research Scientist with The Intervention Center, Oslo University Hospital. His research interests include molecular and nano-neural communications, wireless communications, and positioning in cellular networks. He was awarded the Gold Plaque from the UNIBL for his achievements throughout his undergraduate education.

BIGE DENIZ UNLUTURK (Member, IEEE) received the Graduate degree in electrical and electronics engineering from Middle East Technical University, Ankara, Turkey, in 2011, as a University Valedictorian, the M.Sc. degree from Koc University, Istanbul, Turkey, in 2013, under the supervision of Dr. Ozgur Baris Akan, and the Ph.D. degree in electrical and computer engineering from the Georgia Institute of Technology, Atlanta, GA, USA, in August 2020, under the guidance of Dr. Ian F. Akyildiz. She was a Former Member of BWN at Koc University. In Fall 2021, she started as an Assistant Professor with the Department of Electrical Engineering and the Department of Biomedical Engineering, Michigan State University, where she is currently a Postdoctoral Research Associate with the Dr. Chris Contag's Laboratory, Institute of Quantitative Health Science and Engineering. Her research interests include the areas of wireless communication and networking, more specifically molecular communications and Internet of Bio-Nano Things and their applications to healthcare.

NILOJAN GNANAKULASEKARAN received the master's degree in advanced electronic and electrical engineering from Brunel University London. He is currently attached to The Intervention Center, Oslo University Hospital, as a Research Engineer. His research interests include embedded systems development and wireless communications.

ILANGKO BALASINGHAM (Senior Member, IEEE) received the M.Sc. and Ph.D. degrees in signal processing from the Department of Electronics and Telecommunications, Norwegian University of Science and Technology (NTNU), Trondheim, Norway, in 1993 and 1998, respectively, and the master's degree from the Department of Electrical and Computer Engineering, University of California at Santa Barbara, Santa Barbara, CA, USA. From 1998 to 2002, he was a Research Engineer developing image and video streaming solutions for mobile handheld devices with Fast Search & Transfer ASA, Oslo, Norway, where he is currently a part of Microsoft Inc. Since 2002, he has been a Senior Research Scientist with The Intervention Center, Oslo University Hospital, Oslo, where he heads the Wireless Sensor Network Research Group. He was appointed as a Professor in signal processing in medical applications with NTNU, in 2006. From 2016 to 2017, he was a Professor (by courtesy) with the Frontier Institute, Nagoya Institute of Technology, Japan. He has authored or coauthored more than 200 journals and conference papers, seven book chapters, 42 abstracts, 16 articles in the popular press, and holds negative patents. His research interests include super robust short-range communications for both in-body and on-body sensors, body area sensor networks, short-range microwave sensing of vital signs, short-range localization and tracking mobile sensors, and nanoscale communication networks. He has given 16 invited/keynotes at the international conferences. In addition, he is active in organizing conferences (has also been a Steering Committee Member of ACM NANOCOM, since 2018, the General Chair of the 2019 IEEE International Symposium of Medical ICT, the 2012 Body Area Networks Conference, and the TPC Chair of the 2015 ACM NANOCOM). He is an Editorial Board (has been an Area Editor of *Nano Communication Networks* (Elsevier), since 2013).